Available online at www.sciencedirect.com
ScienceDirect
Journal of Power Sources 161 (2006) 333–345
JOURNAL OF POWER SOURCES
www.elsevier.com/locate/jpowsour

Liquid droplet behavior and instability in a polymer electrolyte fuel cell flow channel

E.C. Kumbur, K.V. Sharp, M.M. Mench *

Fuel Cell Dynamics and Diagnostics Laboratory, Department of Mechanical and Nuclear Engineering, The Pennsylvania State University, University Park, PA 16802, United States

Received 14 February 2006; received in revised form 2 April 2006; accepted 3 April 2006
Available online 9 June 2006

Abstract

A combined theoretical and experimental study of the influence of controllable engineering parameters, including surface PTFE (Teflon™) coverage (ranging from 5 to 20 wt.%), channel geometry, droplet chord length and height, and operational air flow rate, on liquid droplet deformation at the interface of the diffusion media (DM) and the gas flow channel was performed. The theoretical model reasonably predicts the measured contact angle hysteresis and identifies conditions under which the droplet tends toward an unstable state. The results presented in this study indicate that operational conditions, droplet height, chord length, channel size and level of surface hydrophobicity of the DM directly affect the droplet instability. Based on the analytical force balance model, the critical Reynolds number at which a droplet of given dimensions tends towards instability (i.e. may be removed from the channel) is predicted. Experimental data in both the stable and unstable regions as defined by the critical Reynolds number curve generally corresponds to the stability predictions. Empirical correlations relating surface tension and DM PTFE content were developed. At high flow rates, the surface hydrophobicity of the DM surface enhances efficacy of droplet removal, and may help to prevent local channel flooding. However, at low flow rates, hydrophobicity of the DM surface has only a minimal impact on efficacy of droplet removal and therefore high PTFE content may not be necessary, or desirable, since it also increases the electrical resistance of the system. It is also suggested that for constant air velocity and droplet size and shape, reduced channel height is preferred for effective water droplet removal where practical.

Keywords: Flooding; Polymer electrolyte fuel cell; Droplet removal; Gas diffusion layer; Surface tension

1. Introduction

Channel level water transport is a vital issue for maintaining high performance and low parasitic losses in a polymer electrolyte fuel cell (PEFC). Due to the complexity of the thin film porous media and small length scales involved, water transport phenomena in a PEFC are difficult to fully understand. Electrolyte hydration is essential for efficient proton conduction, since its conductivity is a strong function of water content. While the electrolyte membrane needs to be maintained in a fully hydrated condition to ensure high proton conductivity, excess liquid water may hinder the reactant transport to the catalyst sites, a phenomenon generally known as "flooding". Flooding results in high mass concentration losses in the cell and an increase in parasitic pressure losses.

Flooding can be categorized into three types, based on the location of water accumulation. These are: (i) channel level flooding, (ii) diffusion media (DM) flooding, and (iii) catalyst layer flooding. Channel level flooding is commonly observed under low air flow rates, especially in the anode channel at low operating current density [1]. At higher flow rates, the cathode side is more prone to accumulation of excess liquid water, because water is transported from the anode to the cathode by electro-osmotic drag, and electrochemical water generation occurs on the cathode. Excess liquid water transported within the pores of the DM accumulates at the surface of the DM in the channel, forming small droplets. As the DM becomes saturated, these droplets increase in size, eventually coalescing into water slugs in the channel. These water slugs prevent reactants from flowing smoothly in the channel, increasing parasitic pressure loss, and also provide facilitated transport of ionic impurities, which can accelerate the ionomer degradation. On the anode, liquid blockage can cause voltage reduction and fuel starvation to the catalyst layer [2], which can lead to oxidation of car-

* Corresponding author. Tel.: +1 814 865 0060; fax: +1 814 863 4848.
E-mail address: mmm124@psu.edu (M.M. Mench).

0378-7753/$ – see front matter © 2006 Elsevier B.V. All rights reserved.
doi:10.1016/j.jpowsour.2006.04.093

Nomenclature

b	half width of the channel above the droplet, m
B	half width of the channel, m
c	chord length of droplet, m
d_c	hydraulic diameter of the channel, m
F_{drag}	drag force, N
F_P	pressure force, N
F_{shear}	shear force, N
F_{ST}	surface tension force, N
h	droplet height, m
L	total length of the material, m
P_A, P_B	pressure at AA′ and BB′ planes, Pa
r	radius of the droplet, m
R_a	roughness parameter
Re	Reynolds number
u'	average velocity above the droplet, m s^{-1}
y'	centerline of the FF′ plane
U	average velocity in unobstructed channel, m s^{-1}

Greek letters

α	azimuth angle at droplet surface, radian
γ_{sl}, γ_{sv}, γ_{lv}	interfacial tension, (solid–liquid, solid–vapor, liquid–vapor), N m^{-1}
Δ	difference between advancing and receding angle, $\theta_A - \theta_R$, radians (except where noted as degrees)
μ	viscosity of the air, kg m^{-1} s^{-1}
θ_A, θ_R	advancing and receding contact angles, radian
τ	shear stress, N m^{-2}

bon support and accelerated degradation. In order to avoid the partial coverage of the flow channel by liquid water, it is advantageous to understand the droplet behavior at the interface of DM and the flow channel in order to determine the most effective purge strategy. The addition of hydrophobic additive to the DM may enhance water removal, but it also increases electrical and thermal contact resistance between landing and DM, which is undesirable. Therefore, a proper balance between these competing effects must be obtained for the optimal performance.

Due to the complex two-phase flow in the flow channel of PEFC, managing the transport of reactants and products through the flow channels is a challenging issue. The most common way to enhance liquid phase water removal from the channel and improve water management in the DM and catalyst layer is to use hydrophobic gas diffusion media. The naturally hydrophilic carbon fiber DMs are typically tailored by addition of hydrophobic material such as Polytetraflouroethylene (PTFE) during processing. To date, the fraction of hydrophobic additive used is generally determined through inefficient trial-and-error testing. The existing literature [3–5] has also followed a phenomenological approach, and has yet to develop any clear rationale or fundamental knowledge of the basic transport processes of liquid droplets through the DM or at the interfacial boundaries between the DM and the flow channel. Additionally, few modeling or experimental studies on the droplet dynamics and removal at the interface of DM surface and flow channel have been published. There have been a few qualitative direct visualization studies in the flow channel of the actual working fuel cell [6–8], but none have yet provided a fundamental understanding of how the transport of liquid droplets is related to the various parameters, including droplet size, air flow rate, surface tension, and the hydrophobicity of the gas diffusion media.

The contact angle is considered to be a measure of the amount of wetting of the DM by a liquid. It is directly related to the interfacial surface energy of materials; therefore, droplet instability is strongly related to the surface contact angles of the droplet (advancing and receding angle) and surface energy of DM. Several fundamental studies unrelated to fuel cells [9–12] observed the effects of droplet surface adhesion properties such as contact angle hysteresis (the difference between advancing and receding angle), surface tension, and surface roughness on transport phenomena. Even though these studies were not motivated by the problems present in an operational fuel cell, the physical phenomenon of droplet interaction on different surfaces is similar to that occurring in fuel cell flow channels. Dussan et al. [9], Dimitrakopoulos and Higdon [10], Vafaei and Podowski [11] and Lam et al. [12] have performed extensive studies (experimental and theoretical) on liquid droplet behavior over a range of surfaces and conditions. These studies are designed to explain the mechanisms of liquid droplet shear in the presence of the surrounding fluid shear, the displacement of fluid droplets from solid surfaces at different flow rates, the dependence of contact angle on the size of droplets on smooth surfaces, and the effects of liquid properties to contact angle hysteresis. While these studies are very helpful for understanding the droplet interaction on different surfaces, none of them provide sufficient information regarding effective water removal in the fuel cell flow channel under different operating conditions and DM surface hydrophobicities. Recently, Chen et al. [13] proposed a model related to the prediction of the onset of the liquid water droplet instability. This study draws important conclusions on droplet instability, based on a simplified analytical model. Chen et al. [13] concluded that droplet removal can be improved by increasing flow channel length and mean gas flow velocity, or decreasing channel height and contact angle hysteresis. However, there is still much work to be done. Additional parameters that are believed to be important for droplet instability are channel geometry, droplet aspect ratio (height to chord length ratio) and the PTFE surface coverage. This experimental and analytical study is particularly focused on the prediction of the effects of operational conditions and PTFE treatment on the contact angle hysteresis (a measure of droplet instability) of a droplet on the DM surface, in order to discern conditions leading to droplet removal.

2. Theoretical analysis of droplet deformation in shear

An analytical model based on a macroscopic force balance has been developed for a droplet in the flow channel in order to predict the advancing and receding contact angle hysteresis and identify the conditions under which the droplet tends towards an unstable state as a function of engineering parameters.

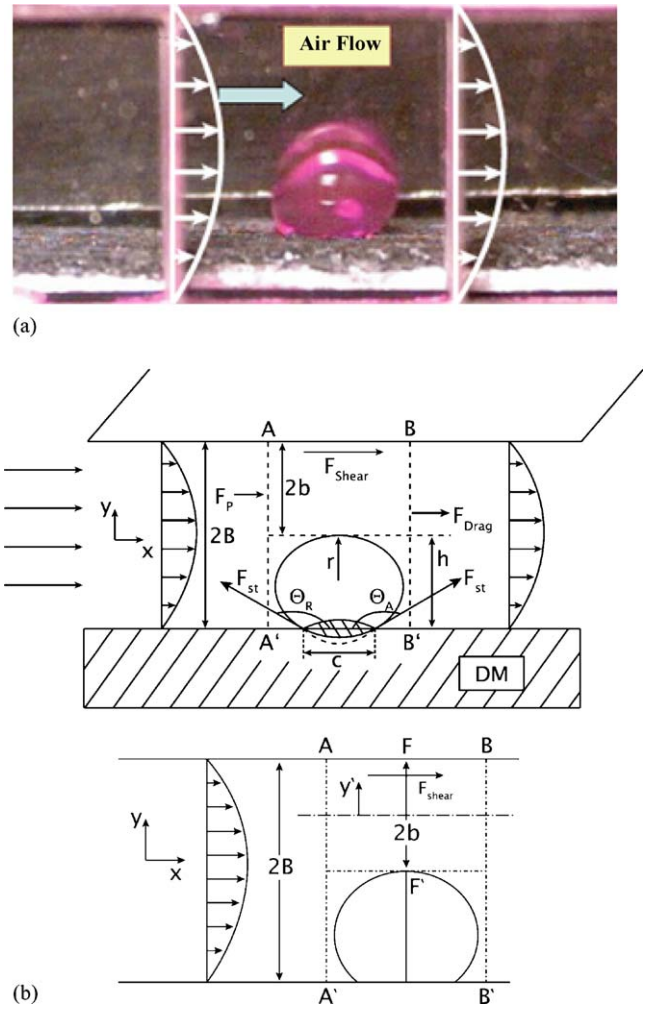

Fig. 1. (a) Captured image of the droplet in the presence of an air shear flow (b) schematic view of control volume chosen for analysis.

Fig. 1 shows a captured image of a droplet on a DM in the experimental flow channel, and schematic view of the control volume chosen, where the droplet starts to emerge on surface of the DM. In the macroscopic force balance model, the air flowing over the droplet is assumed to be Newtonian and incompressible, and the flow in the channel is presumed to be uni-directional, steady, fully developed, and laminar. The droplet is assumed to be spherical.

In Fig. 1, the control volume is defined as AA′BB′ plane, with a depth equal to the diameter of the droplet (into page). The channel height is defined as $2B$, the droplet height is shown as h, and the chord length, or contact length, of the droplet on the DM surface is c. The advancing and receding contact angles of the droplet are given as θ_A and θ_R, respectively. The static macroscopic force balance in the x direction gives:

$$F_{P_x} + F_{\text{shear}_x} + F_{\text{drag}_x} = 0 \tag{1}$$

where F_P represents pressure force created by pressure difference in the flow field, F_{shear} represents the shear force which the fluid exerts on the top wall due to the no slip condition, and F_{drag} is the total drag force exerted on the droplet (equal to the opposite of the surface tension force for a static droplet in equilibrium). The drag force is caused by fluid shear along the droplet surface and it is a function of the flow velocity and pressure gradient. The adhesion force (surface tension force) originates from the molecular interaction of the droplet and the DM surface, and serves to resist the drag force on the droplet through droplet deformation and contact angle hysteresis. If the adhesion force is equal to the drag force, the droplet will not be removed from the channel and the droplet remains at its nucleation point on the DM surface. This stable condition is represented by Eq. (2). Note that in the force balance model, the critical condition is defined as the point, where F_{drag_x} is balanced by F_{ST_x} (surface tension force). Any increase in F_{drag_x} above this critical point represents a condition under which the droplet becomes unstable, thus the critical condition represents a lower bound for droplet removal and defines the point of instability.

$$|F_{\text{ST}_x}| \geq |F_{\text{drag}_x}| = |-(F_{P_x} + F_{\text{shear}_x})| \tag{2}$$

The surface tension force (F_{ST}) is a critical parameter in the force balance equation, since it is directly related to the adhesion tension and surface contact angles of droplets emerging on the gas diffusion media. Assuming that the advancing (θ_A) and the receding (θ_R) angles change linearly along the circumference of the contact surface (wetted surface), a mathematical expression for contact angle on the DM wetted surface can be derived. The wetted surface (contact surface) of the DM is illustrated in Fig. 2. In this force balance model, the shape of the wetted surface (contact surface) is assumed to be circular, thus the diameter of the wetted surface is equal to the chord length of the droplet.

The boundary conditions for the linear contact angle (θ) distribution are: (i) at $\alpha = 0$, $\theta = \theta_A$ and (ii) at $\alpha = \pi$, $\theta = \theta_R$, where all angles are in radians and α represents the azimuthal angle ($\alpha = 0$ represents the advancing edge). Thus the contact angle

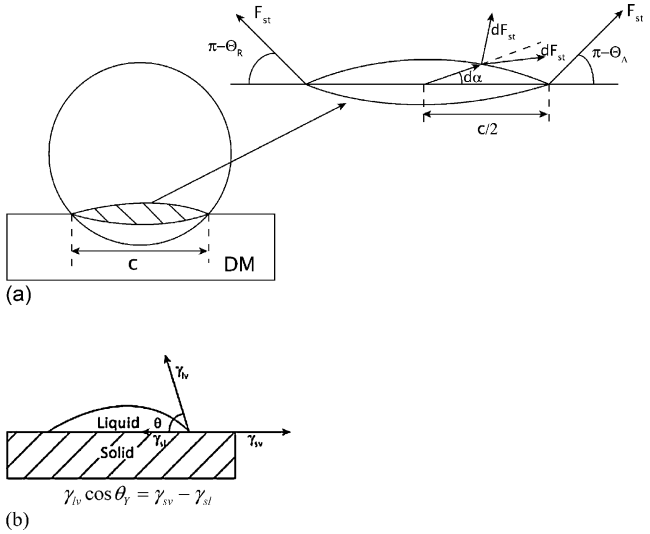

Fig. 2. Schematic view of (a) droplet contact surface, (b) droplet sitting on a surface.

(θ) is defined as:

$$\theta = \frac{-\Delta}{\pi} \cdot \alpha + \theta_A \tag{3}$$

where $\Delta = \theta_A - \theta_R$ represents contact angle hysteresis. The streamwise surface tension force (F_{ST_x}), is calculated by integrating around the wetted perimeter of the DM surface in the streamwise (x) direction. The differential surface tension force in the streamwise direction is, (see Fig. 2);

$$dF_{ST_x} = \left(\gamma_{lv}\frac{c}{2}d\alpha\right)\cos(\pi - \theta)\cos(\alpha) \tag{4}$$

where γ_{lv} represents the surface tension of the liquid vapor interface of water. Performing the integration, the overall surface tension force in the x direction yields:

$$F_{ST_x} = 2\int_0^{\pi} dF_{ST_x} = \gamma_{lv}c\int_0^{\pi} -\cos\left(-\frac{\Delta}{\pi}\alpha + \theta_A\right)\cos(\alpha)d\alpha \tag{5}$$

$$F_{ST_x} = \gamma_{lv}c\frac{\pi}{2}\left[\frac{[\sin(\Delta - \theta_A) - \sin(\theta_A)]}{(\Delta - \pi)} + \frac{[\sin(\Delta - \theta_A) - \sin(\theta_A)]}{(\Delta + \pi)}\right] \tag{6}$$

where Δ represents the difference between the advancing and receding angles ($\Delta = \theta_A - \theta_R$) (note that at the onset of droplet removal or detachment, $|F_{ST_x}| = |F_{drag_x}|$).

Using the simplifying assumption of fully developed laminar flow, pressure drop across the control volume can be calculated in terms of average velocity, droplet chord length, droplet height, and viscosity of the flowing fluid.

The average velocity in the FF′ plane (u') can be related to the average velocity of the air in the channel by applying the conservation of mass relation between the AA′ and FF′ cross sections. Approximating the air as incompressible, $u' = (B/b)U$, where U is the average velocity of the air in the channel before the droplet, u' is the average velocity of the air flow above the droplet, B is the half thickness of the channel and b is the half thickness of the distance between the droplet and top wall of the channel. Based on the fully developed laminar flow assumption in a rectangular channel, the pressure drop across the control volume can be written,

$$P_A - P_B = \frac{3\mu u'}{b^2}2r \tag{7}$$

where P_A and P_B represent the local pressures at the AA′ and BB′ cross sections respectively. Substituting for u' in terms of U, the pressure force acting on the control volume in the x direction then becomes:

$$F_{P_x} = (P_A - P_B) \times \text{area} = (P_A - P_B)2B \times 2r \tag{8}$$

where $2B \times 2r$ represents the cross sectional area of the control volume. Substituting for b in terms of B, ($b = B - h/2$); the pressure force acting on the control volume in the x direction becomes,

$$F_{P_x} = \frac{24\mu B^2 U h^2}{(B - h/2)^3(1 - \cos(\theta_A))^2} \quad \text{where } r = \frac{h}{1 - \cos(\theta_A)} \tag{9}$$

The remaining term in the macroscopic force balance equation (Eq. (1)) represents the shear force (F_{shear}) acting on the control volume. It is assumed that a no slip boundary condition is applicable at the top wall of the control volume. The liquid droplet covers the bottom interface of the channel wall and control volume; therefore it is assumed that there is no air flow through the bottom wall of the flow channel (see Fig. 1). The fully developed laminar flow velocity distribution in a rectangular enclosure in the FF′ plane can be represented by [14]:

$$u(y') = \frac{3u'}{2}\left(1 - \left(\frac{y'}{b}\right)^2\right) \tag{10}$$

where $y' = y + b$ and $y' = 0$ represents the centerline of the FF′ plane. The one-dimensional shear stress in a Newtonian fluid is given as $\tau_{xy} = \mu\, dU/dy$. The shear stress at the top wall ($\tau_{xy}|_{y'=b}$),

$$\tau_{xy}\big|_{y'=b} = -\mu\frac{\partial u}{\partial y'}\bigg|_{y'=b} = \frac{3\mu u'}{b} \tag{11}$$

Substituting u' and b in terms of U and B, the shear force in the streamwise (x) direction at the upper wall of the control volume can be shown as:

$$F_{shear_x} = \tau_{xy}\big|_{y'=b}A = \frac{3\mu BU}{(B - h/2)^2}(2r)^2 \tag{12}$$

Including the derived expressions for the surface tension force (F_{ST_x}), pressure force and shear force terms in the x direction force balance, the final form of Eq. (1) becomes;

$$F_{P_x} + F_{shear_x} + F_{drag_x} = 0 \quad \text{where } F_{drag_x} = -F_{ST_x},$$

$$\frac{24\mu B^2 U h^2}{(B - h/2)^3(1 - \cos(\theta_A))^2} + \frac{12\mu BUh^2}{(B - h/2)^2(1 - \cos(\theta_A))^2} - \gamma_{lv}c\frac{\pi}{2} \times \left[\frac{[\sin(\Delta - \theta_A) - \sin(\theta_A)]}{(\Delta - \pi)} + \frac{[\sin(\Delta - \theta_A) - \sin(\theta_A)]}{(\Delta + \pi)}\right] = 0 \tag{13}$$

The final form of the macroscopic force balance includes a number of engineering parameters, including the surface contact angle hysteresis (Δ, the difference between advancing and receding contact angles), channel flow velocity, droplet height and chord length, and channel height.

3. Experimental methods

In order to observe droplet deformation at the interface of the DM and flow channel, and investigate conditions under which the droplets become unstable (i.e. may be removed by the shear flow), an experimental model cell was fabricated and mounted in a test stand that allowed for precise control of system parameters. While the non-operational model flow channel does not include

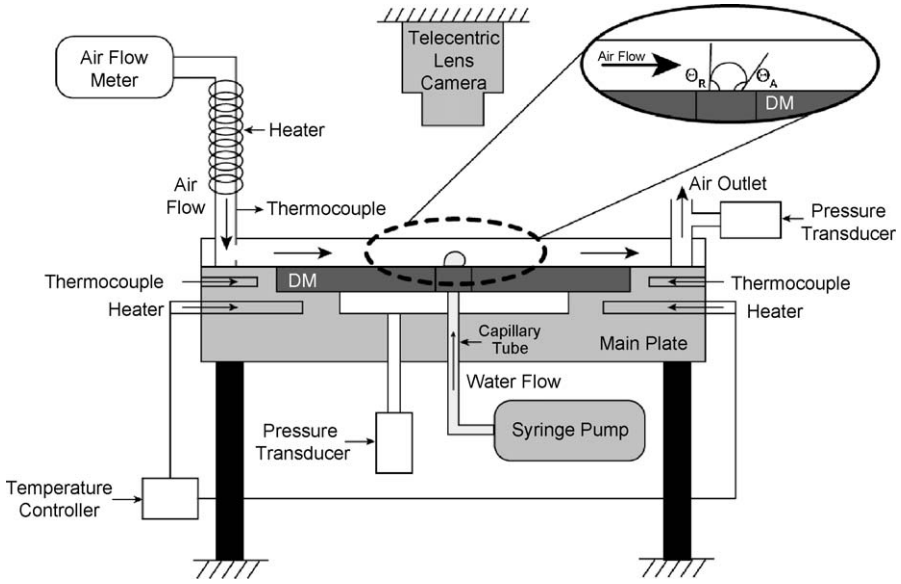

Fig. 3. Schematic view of experimental setup.

electrochemical reaction, it allows simulation of the activity of a cell, and precise visual study of droplet deformation and stability on DM surface, inside the flow channel.

3.1. Method of approach

The hydrogen PEFC flow channel experimental model consists of a rectangular flow channel (5 mm × 4 mm), optically-accessible from the top, with the bottom side consisting of a DM affixed to a feeder plate. A detailed schematic view of the experimental setup is shown in Fig. 3. Three different DMs with controlled hydrophobic treatment were utilized in this study (PTFE content of 5, 10, and 20 wt.%). A controlled liquid flow rate is achieved with a syringe pump apparatus. A combination of a regulator, throttling valve and mass flow meter are used to control and monitor the air flow rate.

The model cell consists of two aluminum end blocks, an aluminum washer, a Lexan™ plate, an aluminum flow channel, prisms, an aluminum settling layer and a hole-pattern feeder plate. The desired flow rate of water simulating the electrochemical water generation is applied through the machined feeder plate by a syringe pump and a capillary tube with a diameter of 0.177 mm. An air flow corresponding to operational fuel cell conditions is externally imposed into the channel through a pressurized gas system and heating system.

Visual images of droplet formation and growth were acquired using a standard video microscopy setup with a telecentric lens and strategically-placed prisms. The prisms (each 5 mm × 5 mm) are aligned on the side walls of the channel in order to enable a simultaneous top and side view of the droplet. The telecentric lens provides an advantage over a conventional lens, in that it mitigates distortion of the shape of small droplets and provides more precise measurements of droplet size and shape. As the liquid droplet formed on the DM surface, images were recorded to allow for measurement of the droplet size and shape.

3.2. Contact angle measurements

Knowledge of surface tension is critical for predicting the conditions under which a droplet may be removed from the channel, since the drag force required for removing a liquid water droplet from the DM surface depends on the interfacial interaction of water molecules and carbon fibers or PTFE on the surface of the DM. However, in the existing literature, indirect approaches are traditionally used to measure the surface tension, due to experimental difficulties [15]. Direct force measurements, contact angles, capillary penetration, sedimentation of particles, and gradient theory are some of the indirect approaches commonly used. Among those, contact measurements are considered to be the easiest way to estimate interfacial surface tensions [16].

The contact angle is a measure of the amount of wetting of the DM by a liquid. It is directly related to the interfacial energy of solid, liquid and vapor phases along the three phase boundary. The contact angles depend both on the base material of surface and surface morphology (roughness). Therefore, investigating the contact angles on different surfaces provides information on the energy of the surface of the interest [16]. However, due to the complexity and small length scale involved in the fuel cell DM, this interface in an enclosed channel is not easily accessible.

Two dynamic contact angles are seen when the liquid droplet is under the influence of air shear flow in the channel. These angles are defined as the dynamic advancing angle and dynamic receding angle (θ_A and θ_R in Fig. 1). These angles could be interpreted as the measure of the ability of the droplet to resist the drag force. The difference between advancing and receding contact angle (contact angle hysteresis, Δ) is a key parameter in determining the adhesion energy and the instability of the droplet which is deformed by the air flow [11–16].

Several experiments were performed to measure the contact angles on the DM with varying PTFE contents under different air flow rates. The porous media used in this experiment was the 200–300 μm thick SIGRACET® Gas Diffusion Layers (SGL

Table 1
Summary of test matrix

Measured parameter	5% PTFE DM at 60 °C, Re = 100–1200 at increment of 100 (15 images at each Re)	10% PTFE DM at 60 °C, Re = 100–1200 at increment of 100 (15 images at each Re)	20% PTFE DM at 60 °C, Re= 100–1200 at increment of 100 (15 images at each Re)
Advancing angle (θ_A)	In each image, measured 5 times	In each image, measured 5 times	In each image, measured 5 times
Receding angle (θ_R)	In each image, measured 5 times	In each image, measured 5 times	In each image, measured 5 times
Chord length (c)	In each image, measured 5 times	In each image, measured 5 times	In each image, measured 5 times
Height (h)	In each image, measured 5 times	In each image, measured 5 times	In each image, measured 5 times

CARBON), which are graphitized carbon fiber-based nonwovens, specifically designed to transport reactant gases into, and excess liquid product water out of, the electro catalyst layers of PEFCs. The DM pore size generally ranges from 50 to 100 μm, although individual surface pore diameter was observed to be as high as to 150 μm. The DM has an uncompressed porosity of 0.84. Three DMs with different level of hydrophobic treatment (PTFE content 5, 10, and 20 wt.%) placed on the feeder side of the assembly were utilized in these experiments. PTFE was assumed to be sprayed homogenously throughout the surface of the DM, although microscopically, variations occur. Contact angles at the interface of three different DMs and gas flow channel were measured at 60 °C at air flow rates ranging from 0 to 5500 ml min^{-1} in increments of 440 ml min^{-1}. Liquid water was injected with a controlled flow rate of 0.023 ml min^{-1} into the DM through the capillary tube with a diameter of 0.177 mm. This water flow rate is used to simulate a current density 1 A cm^{-2} at an equivalent cathode stoichometry of 2 and an active DM surface area of 4 cm^2. Unhumidified air at 60 °C was supplied to the inlet of the flow channel with a controlled flow rate. For each PTFE content, 15 images at each operating Re number (based on channel hydraulic diameter, d_c) were acquired for analysis of the droplet deformation under shear flow. Each image was carefully processed, and advancing and receding contact angles were measured by using IMAGE TOOL® software. Although the high magnification camera and telecentric lens were used to minimize the distortion on each image, each angle was measured five times and then averaged in order to minimize the measurement errors. The measurement error associated with the contact angle measurements was determined to be ±2.8°. A total of 5940 contact angle measurements were made. For each image, the chord length and the height of the droplet were measured and tabulated with contact angle data. The overall test matrix is summarized in Table 1.

4. Results and discussions

4.1. Contact Angle Interpretation

It was expected that contact angle hysteresis ($\Delta = \theta_A - \theta_B$), depends on channel air flow rate (Reynolds number based on channel hydraulic diameter, d_c), droplet size (c and h), and surface treatment of the gas diffusion media (PTFE content) and surface roughness. A functional form of the contact angle hysteresis (Δ) can be written as:

$$\Delta = f(Re, c, h, \text{PTFE\%}, \text{roughness}) \quad (14)$$

Once all the data for three different PTFE cases (5, 10, and 20 wt.%) were collected, the contact angle hysteresis (Δ) versus h/c ratio was plotted at different Reynolds numbers, as shown in Fig. 4. As seen from the Fig. 4, there is scattering in the data, especially at low contact angle hysteresis (Δ). Therefore, a statistical approach was utilized to correlate and understand the behavior of the experimental data. Kwok et al. [15] explained that obtaining meaningful contact angles for the determination of solid surface tensions is a difficult task due to the effects of swelling, chemical composition (inert), and roughness on contact angle measurements, and concluded that statistical tools may help to improve the meaning of measured contact angles to minimize the measurement errors. In Fig. 4, the model output (contact angle hysteresis) was computed by solving the final form of the macroscopic force balance equation (Eq. (13)). Experimental data such as droplet height, droplet chord length, air velocity, viscosity were input into that equation and contact angle hysteresis (predicted Δ) for each droplet size were found. Note that the Reynolds number is not constant across all of the points included in Fig. 4, we know that contact angle hysteresis is a function of Reynolds number. The intent of Fig. 4 is primarily to show the relative agreement between the experimental data, linear regression, and model predictions.

Roughness can be interpreted as the measure of the disturbances on the surface due to the disarrangement and misalignment of the carbon fibers on the DM surface. It is expected that roughness directly affects the line tensions and three phase boundary; therefore it may lead to errors in contact angle measurement and interpretations. Kwok et al. [15] also stated that there is no general criterion to quantify the level at which roughness has a significant effect on contact angle measurements, however in this study, the error in the contact angle measurements induced by roughness can be estimated, based on a typical droplet size (height = 1 mm, chord = 1 mm) and maximum roughness element. As measured from the cross sectional scanning electron microscope (SEM) image of PTFE DM samples, the maximum disturbance on the 20% PTFE DM surface is around 35 μm (Fig. 5), and it was estimated that this maximum roughness results in a ±2° error on contact angle measurements.

A multi-dimensional linear regression model was chosen to correlate measured contact angle hysteresis (Δ) with the relevant non-dimensionalized experimental parameters such as Re, c/d_c and h/d_c, where d_c is the hydraulic diameter of the flow channel. The contact angle hysteresis (Δ) also depends on surface treatment (PTFE content) and, to a minimal extent, surface roughness. However, surface roughness of the DM is not a controlled parameter in these experiments and as discussed,

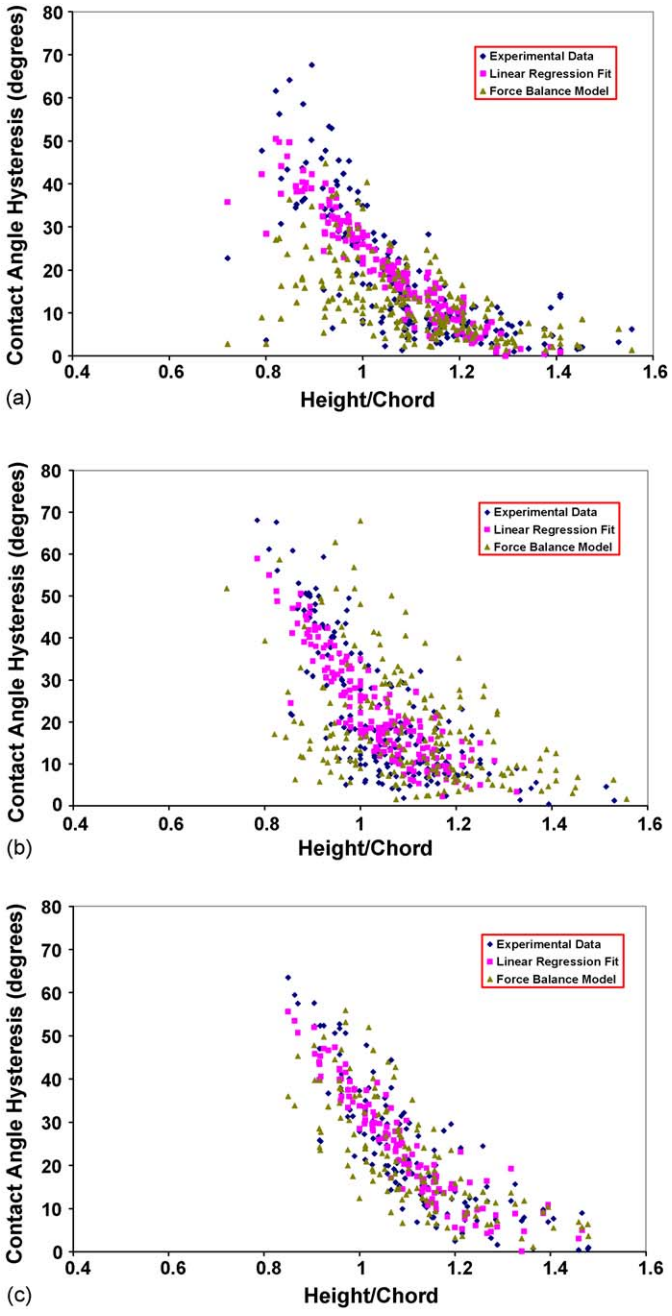

Fig. 4. Comparison of experimental data, linear regression data, and macroscopic force model for three different PTFE regression fits (a) 5% PTFE, (b) 10% PTFE, (c) 20% PTFE.

introduced only a small error in contact angle measurement. Therefore, in our regression model, contact angle hysteresis (Δ) is functionally defined as:

$$\Delta = A + BRe + C\left(\frac{c}{d_c}\right) + D\left(\frac{h}{d_c}\right) \tag{15}$$

The chord length (c) and height of the droplet (h) are non-dimensionelized by d_c, and a different multi-dimensional linear regression model was deduced for each PTFE content. The three multi-dimensional linear regression fits were derived for three different PTFE contents, based on the extensive experimental

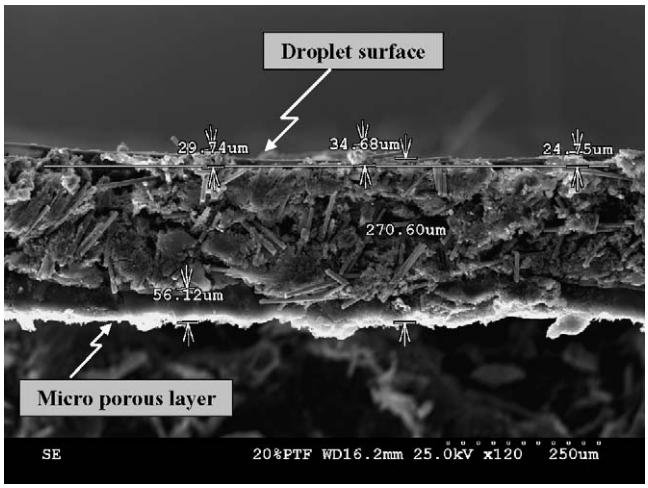

Fig. 5. SEM picture of the cross sectional view of 20% PTFE DM.

data taken. These are:

$$\Delta_{\%5\mathrm{PTFE}} = -11.2 + 0.0156Re + 139\left(\frac{c}{d_c}\right) - 86\left(\frac{h}{d_c}\right), \quad R^2 = 74.1\%$$

$$\Delta_{\%10\mathrm{PTFE}} = 6.02 + 0.018Re + 177\left(\frac{c}{d_c}\right) - 163\left(\frac{h}{d_c}\right), \quad R^2 = 75.1\%$$

$$\Delta_{\%20\mathrm{PTFE}} = -6.52 + 0.0214Re + 145\left(\frac{c}{d_c}\right) - 96.4\left(\frac{h}{d_c}\right), \quad R^2 = 82.1\% \tag{16}$$

The normal plot of residuals, the histogram of residuals, chart of residuals and residuals versus fits were used in order to check the validity of the regression model (i.e. homogeneity of variance, non-independence of variables, normality) as well as to detect outliers in the experimental data. It was noted that the linear regression for contact angle hysteresis (Δ) on prescribed functional form provided an adequate fit to the experimental data. In addition to these regression model diagnostics, the analytical equation (Eq. (13)) derived from the macroscopic force balance analysis was solved for contact angle hysteresis (Δ) by using a Newton Raphson method. Specifically, for each experimental condition, known values of droplet height, droplet chord length, air velocity, viscosity, channel height, and advancing contact angle were input into the final form of the force balance equation along with the experimentally derived values of surface tension. For each case, the contact angle hysteresis (Δ) was predicted and compared to the actual measured contact angle hysteresis (Δ) and values of Δ based on the linear regression fits, and a reasonable agreement between these data was observed. Since contact angle hysteresis depends on air flow rate, droplet aspect ratio (height to chord ratio) and surface treatment of the DM (PTFE content or surface tension), these effects were separately investigated in this study and are reported in the following sections.

4.2. Effect of air flow rate

As shown in Eq. (13), the drag force on the droplet depends linearly on the air flow velocity. As the velocity of the air increases, the drag force increases and the droplet deforms along

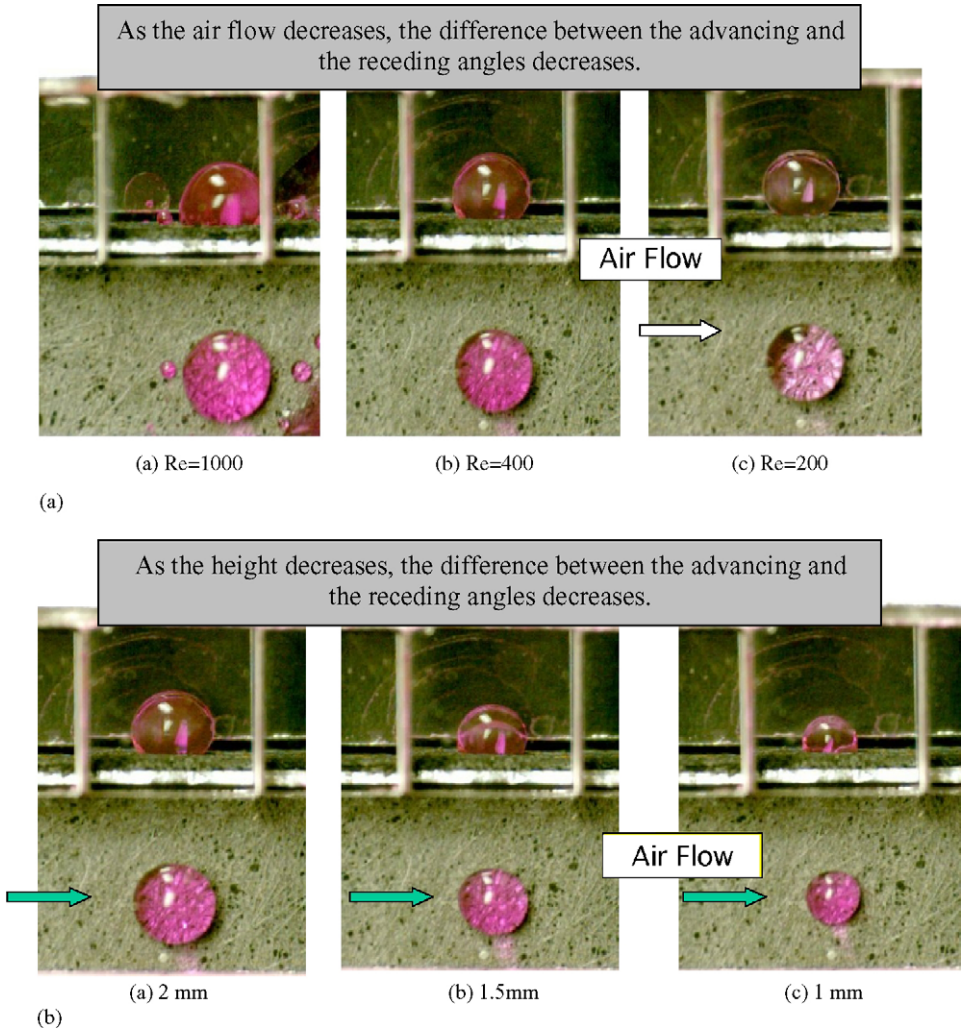

Fig. 6. Captured images of (a) droplets with same height under different air flow rates, (b) droplets with different height under same air flow rate.

the flow direction, causing an increase in contact angle hysteresis (Δ). As flow rate increases, the hysteresis increases and the surface energy (adhesion energy) between DM and water gradually becomes insufficient to resist increasing drag force. As a result, at some point, droplets will detach from the DM surface and will form an annular film, or roll over the DM surface in the direction of flow. The point at which the droplet can no longer resist the drag force is termed the point of instability.

Fig. 6(a) shows a sequence of captured images of the same size droplets under different air flow rates. It can be clearly seen that contact angle hysteresis (Δ) increases with flow rate and the droplet tends towards an unstable condition. To investigate the air flow rate effects on contact angle hysteresis (Δ), contact angle hysteresis (Δ) versus air flow rate was plotted by using the linear regression data for 5%, 10% and 20% PTFE DMs for a specified droplet size (chord length = 1.7 mm and height = 1.9 mm). The macroscopic force balance equation (Eq. (13)) was also solved for contact angle hysteresis (Δ) at the specified droplet size (c = 1.7 mm and h = 1.9 mm) for different air flow rates. The output of the model and linear regression fits for 5% and 20% PTFE DM samples are presented in Fig. 7. Both the force balance model and the regression show that contact angle hysteresis, (Δ) is a linear function of air velocity. As seen from Fig. 7, for each PTFE case, the discrepancy between the model prediction and linear regression is relatively small, which also validates the applicability of applying linear regression fits to the experimental data. As expected, the results shown in Fig. 7 indicate that imposing high air flow rates into the flow channel increases the contact angle hysteresis, thereby causing the droplet to move towards an unstable condition. Thus, imposing high flow rates may enhance the liquid water droplet removal from the flow channel; however, one consequence is that parasitic losses in a fuel cell system also increase with air flow rate.

4.3. Effects of droplet aspect ratio and critical Reynolds number

In this study, it was experimentally observed that the droplet aspect ratio (h/c) has a significant influence on the droplet instability, since any instability is closely related to the balance between the drag force and surface adhesion force, both of which

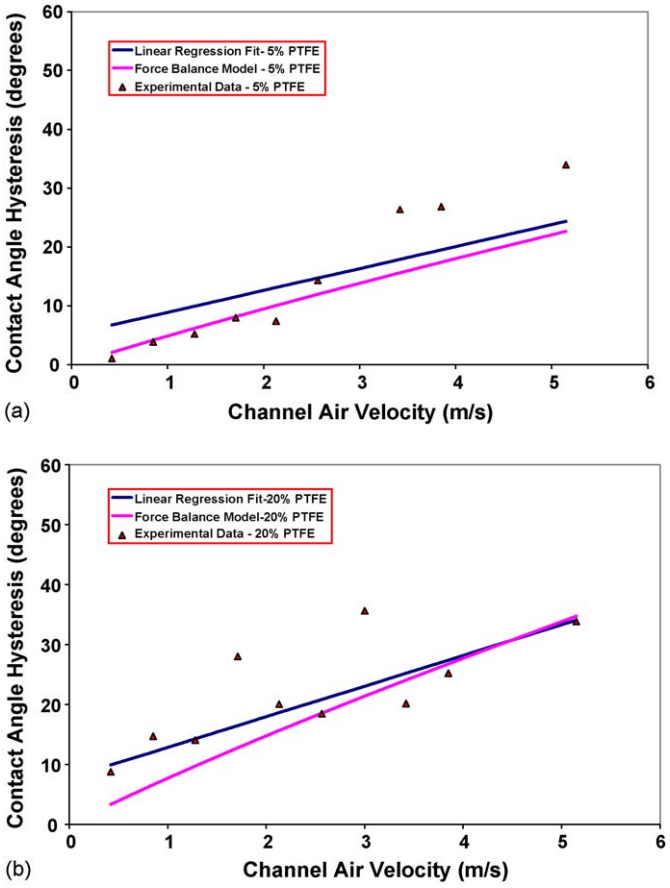

Fig. 7. Contact angle hysteresis (Δ) vs. air velocity for a droplet with constant chord length = 1.7 mm and height = 1.9 mm (a) 5% PTFE, (b) 20% PTFE.

are related to droplet size and shape. Fig. 6(b) shows the captured images of three droplets with different aspect ratios subjected to a constant air flow rate. As seen from Fig. 6(b), the droplets with relatively higher aspect ratio (e.g. taller droplets) deform more in response to the same shear flow. A larger deformation means that the droplet experiences a greater difference between advancing and receding contact angles (Δ) to resist increased drag. As the droplet spreads over the DM surface, its chord length increases more than its height, and the surface tension force (proportional to c) becomes more dominant than the drag force acting on the droplet surface (proportional to h^2). Therefore, the ratio of droplet height to droplet chord length (aspect ratio) is useful in describing droplet behavior.

Using the analytical model based on a macroscopic force balance, the critical Reynolds numbers for which a droplet with specified chord length will be sheared off the surface were determined over a range of droplet aspect ratios and for two specific chord lengths. Reynolds numbers corresponding to the critical condition (onset of detachment) for 5% and 20% PTFE DMs for a droplet with specified chord lengths ($c = 1.9$ and 2.3 mm) versus droplet aspect ratio are shown in Figs. 8 and 9, respectively. The experimental data corresponding to the conditions for which the droplet chord length is 1.9 ± 0.1 mm for 5% PTFE and 2.3 ± 0.1 mm for 20% PTFE, and for which the droplet remained attached on the DM surface are shown in Figs. 8 and 9.

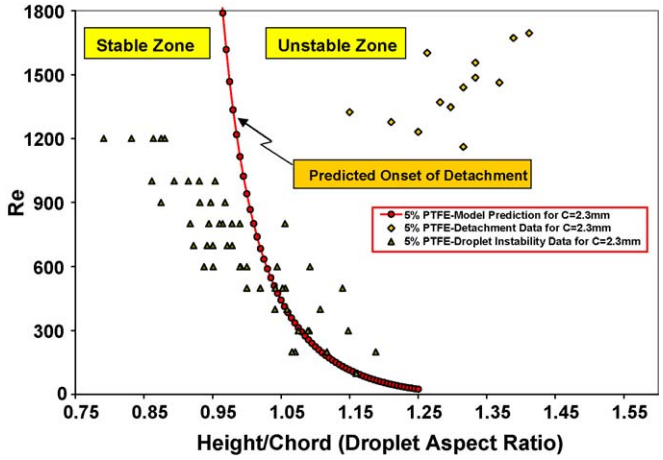

Fig. 8. Critical Reynolds number vs. droplet aspect ratio for a droplet with specified chord length of 2.3 mm on 5% PTFE DM.

Eighty-one percent of the points corresponding to experimental observation of stable conditions lie in the theoretically predicted stable region.

Droplet detachments tests for 5% and 20% PTFE DM samples were also performed. For different droplet aspect ratios, the critical *Re* number leading to droplet detachment are also shown in Figs. 8 and 9. For both 5% and 20% PTFE cases, all the experimental points corresponding to the detachment conditions lie in the theoretically predicted unstable region.

Based on the present model prediction, the Reynolds number required to shear off the droplet is found to increase with decreasing the droplet aspect ratio (height to chord ratio). In other words, any spreading of a droplet (increase in chord length and/or decrease in height) serves to stabilize it and increase the critical *Re* number required for detachment, due to the increased surface adhesion force. Spreading of droplets along the DM surface can eventually lead to the formation of a thin film, which is very difficult to remove regardless of the *Re* number of the imposed gas flow, and which is undesirable for fuel cells. On the other hand, relatively taller droplets (higher aspect ratio) are

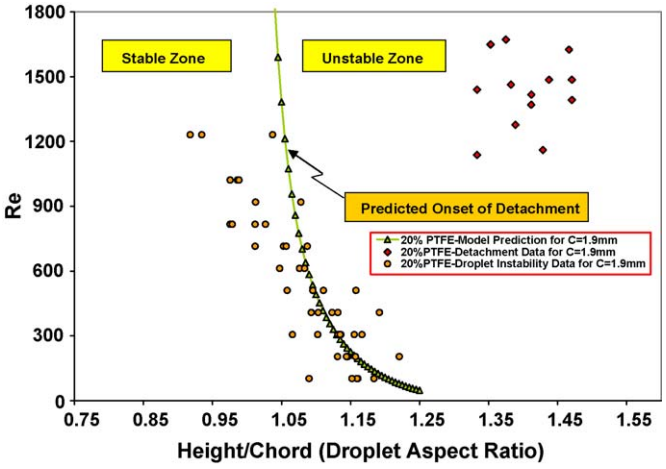

Fig. 9. Critical Reynolds number vs. droplet aspect ratio for a droplet with specified chord length of 1.9 mm on 20% PTFE DM.

easier to remove (lower critical *Re*), since larger frontal area gives rise to a relatively larger drag force. The greater drag force causes a larger difference between advancing and receding angle (contact angle hysteresis, Δ) hence the droplet becomes more unstable.

As expected, at a specified droplet aspect ratio, the droplet on the 5% PTFE DM requires a higher critical *Re* number for detachment than the DM with 20% PTFE content, since higher PTFE content reduces the surface adhesion force. Thus growth of the droplet in the cross stream direction (in *y* direction) rather than in the streamwise (*x*) direction is desirable. Hence the surface hydrophobicity of the DM should be tailored such that it discourages droplet growth in the streamwise direction, since streamwise spreading leads to a stable condition. Spreading in any direction also increases the probability of coalescing of the multiple droplets due to the increased surface coverage of droplets, which in turn may lead to local channel flooding and a stable annular flow film in the channel, the least desired outcome.

4.4. Surface tension calculations as a function of PTFE content

The surface tension components of the DM, air, and liquid droplet system have been estimated based on measured data. For a static system, solid surface interfacial tensions can be calculated from the measured contact angles using the mechanical equilibrium relation published by Young in 1800 [17]. The liquid droplet contact angle on any solid surface can be defined by the mechanical equilibrium of the droplet under the action of three interfacial tensions, including solid surface tensions [15]. Fig. 2 represents the schematic view of the liquid droplet sitting on a solid surface, where γ_{lv}, γ_{sl} and γ_{sv} represent the liquid–vapor, solid–liquid and solid–vapor surface tensions respectively. A simple force balance on the droplet contact surfaces in the *x* direction gives the surface tension components of the solid material.

Since the macroscopic force balance model requires a value of solid surface tensions, Young's relation [17] was used in conjunction with the experimental linear regression fits, in order to define the surface tension forces of the tested DMs with 5%, 10%, and 20% PTFE content. Substituting the liquid–vapor surface tension term in terms of solid–liquid, solid–vapor and contact angle into the previously derived form of the macroscopic force balance equation (Eq. (13)), a final version of the force balance equation becomes:

$$\frac{24\mu^2 B^2 Reh^2}{(B-h/2)^3(1-\cos(\theta_A))^2\rho d_c} + \frac{12\mu^2 BReh^2}{(B-h/2)^2(1-\cos(\theta_A))^2\rho d_c} - \frac{(\gamma_{sv}-\gamma_{sl})}{\cos\theta_A} c\frac{\pi}{2}\left[\frac{[\sin(\Delta-\theta_A)-\sin(\theta_A)]}{(\Delta-\pi)} + \frac{[\sin(\Delta-\theta_A)-\sin(\theta_A)]}{(\Delta+\pi)}\right] = 0 \quad (17)$$

Substituting the three different linear regressions fits (derived from the experimental data for 5%, 10%, and 20% PTFE content) into Eq. (17) with *U*, *c*, *h* terms from the experimental data for each PTFE content, one can solve the equation for the surface tension terms ($\gamma_{sl}-\gamma_{sv}$) term for each PTFE content. Surface tension terms ($\gamma_{sl}-\gamma_{sv}$) were tabulated for each different PTFE value and shown in Table 2.

Table 2
The model prediction of surface tension terms ($\gamma_{sl}-\gamma_{sv}$) for different DM

The amount of PTFE surface coverage of DM (wt.%)	The difference between solid–liquid and solid–vapor interfacial tensions of DM ($N\,m^{-1}$) (model prediction)
5% PTFE	$\gamma_{sl}-\gamma_{sv}=0.02516$
10% PTFE	$\gamma_{sl}-\gamma_{sv}=0.02004$
20% PTFE	$\gamma_{sl}-\gamma_{sv}=0.01562$

To date, empirical studies have been inconclusive regarding the best DM structure for two-phase flow management at the channel level, and to the authors' knowledge, no empirical correlation relating the surface tension to the PTFE coverage of DM has been reported. Eq. (18) represents the linear regression fit (Fig. 10) showing the solid surface tensions ($\gamma_{sl}-\gamma_{sv}$) of the DM in terms of PTFE content. As anticipated, the surface tension values decrease as the PTFE content increases, assuming all other parameters are held constant. The adhesion force on a droplet decreases as well. Thus, as expected, droplet removal is facilitated under a higher PTFE loading.

$$\gamma_{lv}\cos\theta_A = \gamma_{sv}-\gamma_{sl} = 0.0006\,(\%\,\text{PTFE}) - 0.0274,\quad R^2 = 0.95\,(N\,m^{-1}\ \text{at}\ 60\,^{\circ}C) \quad (18)$$

The linear equation relating ($\gamma_{sl}-\gamma_{sv}$) and PTFE content (Eq. (18)) may be used to estimate surface tension values over the range of 5–20% PTFE loadings, although an asymptotic approach for high PTFE loadings is expected over the entire range. In order to validate the surface tension values found by the force model, solid surface tension terms were compared to literature. The surface tension component approach and equation of state approach are known to be the two basic models used to find values γ_{sl} and γ_{sv} separately [16]. Kwok et al. [15] provided a FORTRAN program to calculate the solid–liquid and solid–vapor interfacial tensions (γ_{sl}, γ_{sv}) by solving the equation of state. Using this code, the equation of state was computed

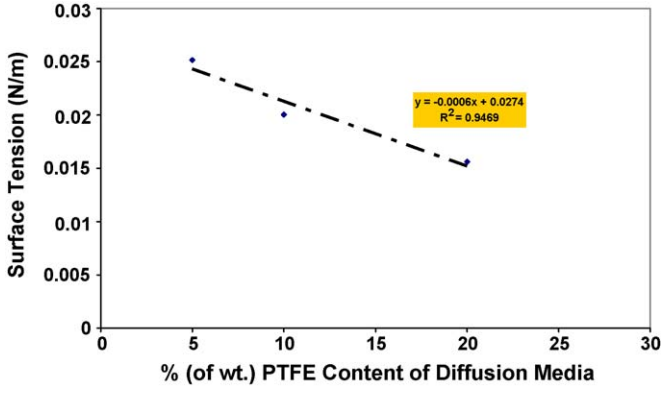

Fig. 10. Solid surface tension difference ($\gamma_{sl}-\gamma_{sv}$) of DM vs. % PTFE content of DM.

Table 3
Calculated solid–vapor (γ_{sv}), and solid–liquid (γ_{sl}) surface tensions of different DM

Amount of PTFE (wt.%)	Solid–vapor tension, γ_{sv} (N m^{-1}) at 60 °C	Solid–liquid tension, γ_{sl} (N m^{-1}) at 60 °C
5% PTFE	0.00636	0.03152
10% PTFE	0.00805	0.02809
20% PTFE	0.00967	0.02529

and three different values of γ_{sv} and γ_{sl} for each PTFE content were found and listed in Table 3.

When these values are compared to Zisman et al. [18], excellent agreement is reached. The average value of all three γ_{sv} is 0.008 N m^{-1} at 60 °C. Zisman et al. [18] calculated the solid–vapor interfacial tensions for different materials by using experimental static contact angles with the equation state approach. He found a solid–vapor interfacial tension (γ_{sv}) value of PTFE of 0.018 N m^{-1} with a static contact angle 108°. When this value is compared to the value predicted by the present macroscopic force balance model, it is seen that the model prediction and Zisman's prediction are at the same order of magnitude; however, the force balance model predicts the value γ_{sv} slightly lower than the Zisman et al. [18], due to the dependence of surface tension on temperature. The present model predicts the solid–vapor surface tension of DM at 60 °C, however, Zisman et al. [18], listed the solid surface tension values of the materials at 20 °C. The discrepancy between these values arises due to the fact that as the temperature increases, the molecular interaction at the interface increases, hence molecules behave more independently due to the excess stored kinetic energy. As a result of this, adhesion forces decreases.

4.5. Impact of PTFE content

4.5.1. Contact angle hysteresis

The macroscopic force balance model was solved for contact angle hysteresis for three different PTFE samples of SGL® carbon paper in order to obtain a reasonable estimate of the droplet instability as a function of PTFE content. Contact angle hysteresis (Δ) versus channel air velocity at a specified droplet chord length (c = 1.7 mm and h = 1.9 mm) and different PTFE loading DMs is shown in Fig. 11. At a specified air velocity, the maximum contact angle hysteresis occurred in DM with 20% PTFE content and minimum contact angle hysteresis occurred in DM with 5% PTFE content. Physically, the surface adhesion force is reduced by rendering the DM surface more hydrophobic. As a result, at higher PTFE loadings of the DM (decreased adhesion energy of the water molecules onto the treated carbon fiber), the droplet deforms more readily, causing high contact angle hysteresis. Hence, the liquid water droplets located on a high PTFE loading surface tend to be more unstable, and the drag force required to remove the water droplets of a given size decreases.

4.5.2. Flow rate effects

The two primary parameters affecting the droplet instability are PTFE content and air flow rate. However, in order to develop a new design criterion for effective water removal from the flow channel, an optimal balance between the amount of PTFE content of the DM and air flow rate must be considered. Engineering consequences of increasing PTFE content and air flow rate include the material cost, electrical resistance of the DM increase as the amount of PTFE content increases, and increased parasitic losses due to the increase in air flow rate.

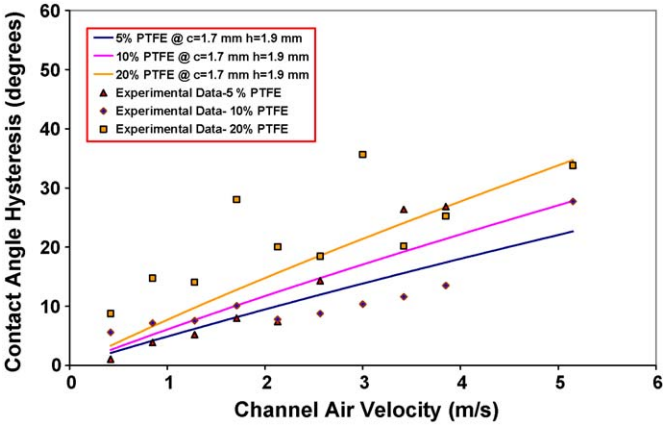

Fig. 11. Contact angle hysteresis (Δ) vs. air velocity at h = 1.9 mm and c = 1.7 mm for three different PTFE contents (model prediction).

To assess the relative significance of PTFE content and air flow rate on the stability of the droplet, the variation in contact angle hysteresis on different PTFE content of the DM was compared at different air flow rates using the macroscopic force balance equation. Using the experimentally-correlated surface tension values for each PTFE content, the force balance equation was solved for the contact angle hysteresis (Δ) and air velocity at a constant chord length and height (c = 1.7 mm and h = 1.9 mm), shown in Fig. 11. A linear functional dependence between the contact angle hysteresis (Δ) and air velocity was also observed, although there was some scatter. Note also that the difference in the predicted Δ between each PTFE value diverges as the velocity of the air increases in the channel; however, at low velocity, the difference in Δ between three PTFE contents is almost negligible.

The dependence of contact angle hysteresis (Δ) on PTFE content of the DM, over a range of Reynolds numbers has also been investigated using the analytical force balance model, as shown in Fig. 12. It is observed that increasing the PTFE content for low Reynolds number does not change the contact angle hysteresis significantly, but for Reynolds numbers greater than 600, increases in PTFE content do significantly impact contact angle hysteresis (Δ). Effectively, the influence of PTFE content on contact angle hysteresis is more dominant in the high air flow rate (Reynolds number) regime. However, under low air flow conditions, water removal from the channel is relatively unaffected by the surface PTFE content, and therefore high PTFE content is not necessary, or desirable since PTFE additive will have the additional effect of increasing thermal and electrical contact resistance. Therefore, it can be concluded that using higher PTFE content DMs only enhances the water droplet removal from channels significantly under higher Reynolds numbers.

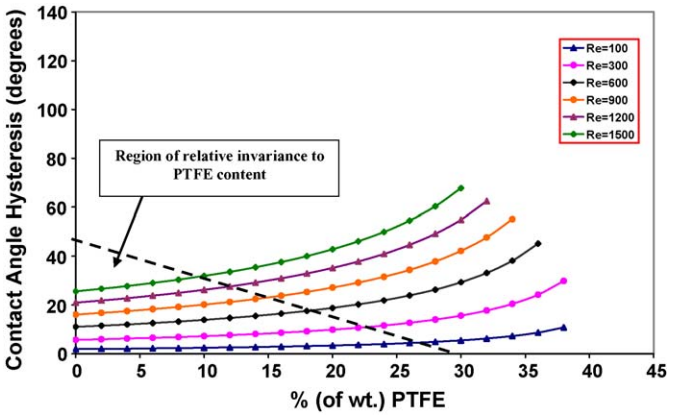

Fig. 12. Contact angle hysteresis (Δ) vs. % PTFE surface coverage (Model prediction) for a droplet with $c = 1.7$ mm and $h = 1.9$ mm.

4.6. Effect of channel height

Eq. (13) was solved for contact angle hysteresis (Δ) in order to predict the effect of channel aspect ratio on droplet hysteresis. The contact angle hysteresis was predicted for a droplet with constant dimensions ($c = 0.5$ mm, h=0.5 mm) over a range of different channel heights (Fig. 13). As shown in Fig. 13, for a constant droplet size and average flow velocity over all PTFE contents, the contact angle hysteresis (Δ) is reduced as the channel itself becomes taller (increasing height), resulting in a more stable condition for the droplet. Physically, since $\Delta P \sim U^2/d_c$, for a constant droplet size and average flow velocity, as the channel gets taller (with no corresponding change in width), the pressure required to drive the flow at that given velocity decreases, reducing the pressure force on the droplet, thus decreasing the acting drag force.

For the varying channel heights shown in Fig. 13, contact angle hysteresis (Δ) is affected more strongly by PTFE content at the higher average flow velocity ($U = 8.5$ m s^{-1}, $Re = 760$–2030). Specifically, in the force balance model, for average air velocities of 2.13 m s^{-1} ($Re = 190$–507) and below, the variation in contact angle hysteresis (Δ) over all PTFE tested is less than 5° and can be considered negligible for this lower range of average flow velocities.

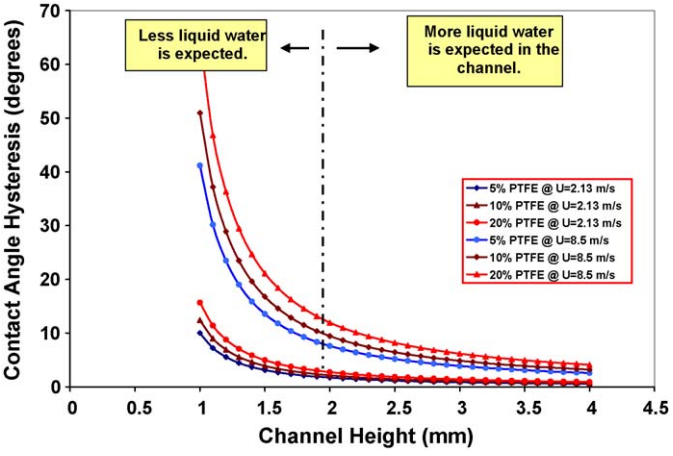

Fig. 13. Contact angle hysteresis (Δ) vs. channel height (mm) for a constant droplet size ($c = 0.5$ mm and $h = 0.5$ mm) at different average air velocities (model prediction).

In summary, the present model predicts that, in the absence of wall interactions, and for constant air velocity, droplet size, and PTFE loading, the lowest tolerable channel height within the limits of other constraints provides the most efficient water droplet removal from the flow channel. Within the set of parameters considered in the current study, the model predicts that the best water removal can be achieved in flow channels having the shortest height, at high average air velocities ($U > 2.13$ m s^{-1}), and with 20% PTFE loading of DM. Liquid water accumulation and residual water content in the flow channels and diffusion media for different flow-field geometries were also investigated by Turhan et al. [19]. Using neutron imaging, they reported that channel water content increased with increasing the channel aspect ratio, in agreement with the present results. They concluded that there can be large differences in the stored water content which is a function of channel geometry [19].

5. Conclusions

Data on surface droplet deformation and removal from a fuel cell diffusion media (DM) surface was determined by employing simultaneous visualization of both the top and side views of a water droplet under an imposed shear flow. Additionally, an analytical force balance model was derived to show the droplet instability boundary in shear flow. Since numerical values for surface tension of a droplet on DM as a function of PTFE content are not available in the literature, an empirical correlation of surface tension versus PTFE content was developed based on the experimental data. Overall, the theoretical and experimental data agree reasonably well. It was observed that channel flow rate, droplet chord length and height, channel geometry, and surface properties of gas diffusion media such as hydrophobicity directly affect the degree of droplet deformation, and therefore influence droplet removal. As expected, imposing high air flow rates into the flow channel increases the contact angle hysteresis, promoting droplet removal. Other specific conclusions that can be drawn for this study include:

(i) The removal of the relatively taller droplets (higher aspect ratio) is easier than that of relatively spread out droplets and films, due to the squared dependence of the drag force acting on the droplet on height, and the linear dependence of the surface adhesion force on droplet chord length.

(ii) Using higher PTFE loadings of the DM promotes increased deformation of the droplet, causing higher contact angle hysteresis, due to the decreased surface interfacial tensions of the water molecules onto the carbon fibers. In addition, the influence of PTFE content on contact angle hysteresis is more important in a high air flow rate regime ($Re \geq 600$). Under a low air flow condition, droplet instability (and removal) is unaffected by the surface PTFE content, and so at low air flow rate operations such as in an anode, high PTFE content is not necessary, or desirable, since increased surface PTFE increases electrical resistance and material cost.

(iii) Given a constant droplet size and constant channel width, the lowest channel height is found to be the most effective for droplet removal, in the absence of channel-wall interactions.

This study can be useful for optimal selection of the PTFE content of the gas diffusion media and determination of operating conditions and channel design for effective channel water slug removal.

Acknowledgements

This research is supported by NSF Grant # CTS-0414319. The authors would like to thank M. Edson, S. O. Ural, M. Khandelwal, S. Y. Yoon, E. Corbin and T. Chorman for their help during this study. The authors are also grateful to Dr. K. S. Chen and Dr. U. Pasaogullari for their helpful comments and discussions.

References

[1] N. Pekula, K. Heller, P.A. Chuang, A. Turhan, M.M. Mench, J.S. Brenizer, K. Ünlü, Nucl Instrum. Methods Phys. Res. Sect. A: Acc., Spectrom., Detect. Assoc. Equip. 542 (2005) 134–141.
[2] C.A. Reiser, L. Bregoli, T.W. Patterson, J.S. Yi, J.D. Yang, M.L. Perry, T.D. Jarvi, Electrochem. Solid State Lett. 8 (2005) A273–A276.
[3] C. Lim, C.Y. Wang, Electrochim. Acta 49 (2004) 4149–4156.
[4] G.G. Park, Y.J. Sohn, T.H. Yang, Y.G. Yoon, W.Y. Lee, C.S. Kim, J. Power Sources 131 (2004) 182–187.
[5] L.R. Jordan, A.K. Shukla, T. Behrsing, N.R. Avery, B.C. Muddle, M. Forsyth, J. Power Sources 86 (2000) 250–254.
[6] K. Tüber, D. Pocza, C. Hebling, J. Power Sources 124 (2003) 403–414.
[7] X.G. Yang, F.Y. Zhang, A.L. Lubawy, C.Y. Wang, Electrochem. Solid State Lett. 7 (2004) A408–A411.
[8] H.S. Kim, T.H. Ha, S.J. Park, K. Min, M. Kim, ASME Paper No. FUELCELL 2005-74113 (2005).
[9] V.E.B. Dussan, J. Fluid Mech. 151 (1985) 1–20.
[10] P. Dimitrakopoulos, J.J.L. Higdon, J. Fluid Mech. 435 (2001) 327–350.
[11] S. Vafaei, M.Z. Podowski, Nucl. Eng. Des. 235 (2005) 1293–1301.
[12] C.N.C. Lam, N. Kim, D. Hui, D.Y. Kwok, M.L. Hair, A.W. Neumann, Colloids Surf. 189 (2001) 265–278.
[13] K.S. Chen, M.A. Hickner, D.R. Noble, Int. J. Energy Res. 29 (2005) 1113–1132.
[14] F.M. White, Fluid Mechanics, 4th ed., McGraw-Hill Series in Mechanical Engineering, 1999, pp. 357–362.
[15] J. Kim, MS Thesis, The Pennsylvania State University, College of Engineering, 2002.
[16] D.Y. Kwok, A.W. Neumann, Adv. Colloid Interface Sci. 81 (1999) 167–249.
[17] T. Young, Philos. Trans. Soc.: London (1805) 9565.
[18] W.A. Zisman, Adv. Chem. Ser.: Am. Chem. Soc. 43 (1965).
[19] A. Turhan, P.A. Chuang, K. Heller, J.S. Brenizer, M.M. Mench, T. Trabold, Liquid water distribution and flooding as a function of flow field design in a PEFC, in: Presented at the 208th Electrochemical Society Meeting, Los Angeles, California, 2005.